ON THE ELECTRO-HYDRODYNAMIC FLOW-FIELD IN ELECTROSTATIC PRECIPITATORS

Hans-Joachim Schmid
Lehrstuhl für Feststoff- und Grenzflächenverfahrenstechnik
Technische Universität München · D-85748 Garching, Germany

Steffen Stolz
Institut für Fluiddynamik
ETH Zürich · ETH Zentrum · CH-8092 Zürich, Switzerland

Hans Buggisch
Institut für Mechanische Verfahrenstechnik und Mechanik
Universität Karlsruhe · D-76128 Karlsruhe, Germany

ABSTRACT

In this paper electro-hydrodynamic (EHD) flows are investigated theoretically with results presented for the flow field in model electrostatic precipitators (ESP's). The resulting flow field is shown and explained qualitatively. Calculations with a k-ε-model show the influence of the mean flow velocity and the importance of the inhomogeneity of the electric field distribution at the inlet and outlet of an ESP. Furthermore a perturbation analysis is presented, leading to a simple differential equation of the Helmholtz type. This allows a more detailed view of the important mechanisms which form the secondary flows as well as a means to get a very fast estimation of the resulting flow field.

INTRODUCTION

A number of technical devices exists with flows characterized by an ionic current transferring momentum into the fluid, e.g. corona chargers, toner application, powder lacquering, electrostatic precipitators (ESP) etc. Since the flow field is modified by electrical phenomena, it is denoted an 'electro-hydrodynamic (EHD) flow'.

This paper is dealing with the EHD-flow in ESP's. Electrostatic precipitators are very important industrial devices for cleaning large amounts of particle laden gas. The functional principle is based on the unipolar charging of the particles in a corona discharge and withdrawing them from the gas flow by means of an electric field.

A wire-duct electrostatic precipitator is the most frequently used type in industry. It consists of parallel plates which form a series of ducts. Within each duct there is a row of wires (fig. 1). When high voltage is applied to the wires, a corona discharge takes place. This process generates ions, resulting in a current flow from the discharge wires to the plates, whereby the particles are charged and hence transported by the electric field towards the collecting plates (White 1963).

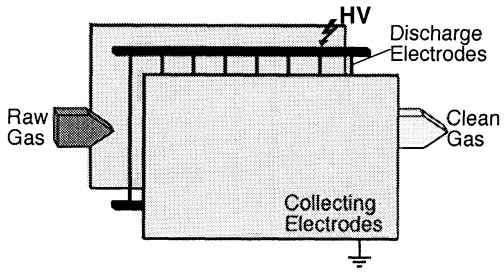

Figure 1. Sketch of a single duct of an Electrostatic Precipitator

ESP's are widely used in industry and a number of investigations have been performed during the last decades. However, sizing a new precipitator is still an empirical matter and many questions concerning the physical phenomena taking place in the precipitator still remain unsettled. One very important question to predict particle transport in ESP's is the knowledge about the flow field.

This topic was examined in several reports with partially contradictory results and few help to predict how the flow field is influenced by a specific design of an ESP. E.g. Ramadan and Soo (1969) as well as Yamamoto and Velkoff (1981) performed calculations, neglecting turbulent velocity fluctuations. Subsequently a number of authors show results of standard k-ε-model calculations for different geometries and operating conditions, e.g. Bernstein and Crowe (1979), Kallio and Stock (1992), Liang and Lin (1994), Choi and Fletcher (1997), Medlin et al. (1998). Recently Soldati and Banerjee (1998) published some DNS calculations of an EHD flow.

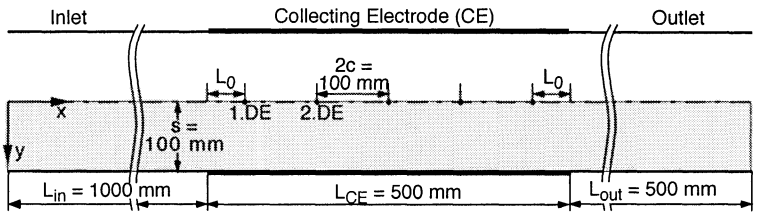

Figure 2. Sketch of model precipitator gap. Calculation domain grey shaded.

This paper aims to clarify the physics and mechanisms of EHD flows, leading to a better understanding, how extensive deteriorations of the flow field could be avoided by a proper design and arrangement of electrodes as well as a proper choice of operating conditions.

MODELING APPROACH

Geometry of Model-ESP

The numerical studies were performed for a two-dimensional model precipitator gap as sketched in fig. 2. It consists of two flat, conducting plates acting as collecting electrodes and a row of five equidistant wires as discharge electrodes. The plate-to-plate spacing was assumed to be 200 mm, a value often used for laboratory scaled precipitators and similar to those of commercial ESP's. The length of the collecting electrodes amounts to 500 mm.

Although the shape of commercially used discharge electrodes vary greatly smooth wires were used for this numerical study, because this electrode type is often used for lab-scaled ESP's. Furthermore for smooth wires the electric field is supposed to be two-dimensional, which simplifies these calculations without loss of generality regarding the physical mechanisms of ionic wind generation. Although a turbulent flow is always three-dimensional, the mean flow field can be considered as two-dimensional, however.

Due to the symmetry of the arrangement, always only one half of the precipitator gap is modeled (grey shaded in fig. 2) and displayed in any following figure.

Modeling of Electric Field

If steady–state discharge is assumed the distribution of the electric potential Φ is governed by the Poisson equation, with the inhomogeneity containing the ion ρ_I and particle space charge ρ_P respectively and the electric permittivity ε_0:

$$\Delta\phi = -\frac{\rho_I + \rho_P}{\varepsilon_0} \tag{1}$$

In addition the conservation of space charge must be met:

$$div\vec{j}_I = 0 \tag{2}$$

Since electric fields are quite strong inside ESP's the transport of ions may be treated as merely due to electrostatic forces. Therefore the current flux j_I may be modeled with a mobility of the ions b_I and the electric field strength E:

$$\vec{j}_I = \rho_I b_I \vec{E} \tag{3}$$

At the discharge wires and the collecting plates Dirichlet boundary conditions are prescribed. Neumann boundary conditions were applied at the symmetry line and at the inlet and outlet far from the wires where the field is approaching zero. At the wall preceding and following the collecting electrode (called 'inlet' and 'outlet') also Neumann boundary conditions were assumed simulating the charge accumulated on the acrylic glass walls where no field lines are ending any more (Schmid, 1999).

The calculations were performed solving eq. 1 with a finite element method and eq. 2 with a finite volume method iteratively (Meroth, 1997).

Flow-Field Modeling

EHD-coupling. Since the ions represent only a very small fraction of the fluid molecules (approximately 10^{-11}) they will transfer their energy captured in the electric field with each collision to the neutral fluid. Therefore the impact of the electric field on the fluid flow can be considered as a volume force f_{el}:

$$\vec{f}_{el} = \rho_I \cdot \vec{E} \tag{4}$$

Statistical Turbulence Model. In order to model the turbulent flow field RANS calculations with a standard k-ε-model (Launder and Spalding 1974, Launder et al. 1975) were performed. The volume force calculated according to eq. 4 is included in the momentum equations.

If the volume force is included in the derivation of the transport equations for the turbulence quantities k and ε, they contain further correlations of velocity and volume force fluctuations. In respect of the lack of a proper modeling approach, these terms were assumed to equal zero.

The numerical scheme uses a finite volume scheme on a structured grid with boundary fitted coordinates allowing an accurate modeling of the discharge electrodes. In regions of high gradients of either electric or flow field the mesh was refined. As solver the commercially available code FLUENT was used, extended by the implementation of the electric body forces (eq. 4).

Perturbation Analysis. In order to obtain a better understanding of the physical phenomena governing the EHD

flow a perturbation analysis of the two-dimensional non–viscous Navier–Stokes equations for a stationary, incompressible and fully developed flow is performed: The mean values of velocities, pressure and volume force are decomposed in one part as it would be without an applied electric field and consequently body force (denoted by capital symbols) and one part as perturbation caused by the influence of the electric field (denoted by an asterisk), e.g.:

Velocity in mean flow direction: $u = U + u^*$

Velocity perpendicular to the wall: $v = V + v^* = v^*$

These decompositions are inserted into the two-dimensional NS–equations and the conservation equation of mass. All perturbations are assumed to be small compared with the main flow. Therefore all products of perturbation quantities are omitted. This implies the constriction to main flow velocities significantly higher than electrically induced secondary flows. Hence this analysis can be interpreted as the limiting case of 'infinite convection'.

Finally one obtains a Helmholtz differential equation in the perturbation of velocity perpendicular to the wall v^*. The inhomogeneity contains the electric body force f and the curvature of the main flow velocity profile:

$$U\Delta v^* = -\frac{1}{\rho}\left(\frac{\partial f_x}{\partial y} - \frac{\partial f_y}{\partial x}\right) + v^*\frac{\partial^2 U}{\partial y^2} \qquad (5)$$

If the electric forces and the main flow field is known, eq. 5 is of the same type as eq. 1 which determines the electrical potential and may therefore be solved very easily. It would be even possible to solve equations 5 and 1 with the same solver simultaneously.

Furthermore the equation itself manifests some interesting aspects of the EHD flow properties without any numerical calculations:

1. The secondary flow depends on *derivatives* of the volume force. This is especially important for the modeling of the electric potential, because this term depends on the second derivative of the potential, therefore requiring very high accuracy of the modeled electric potential to get reasonable fluid flow calculations. 2. If the second term on the right–hand side is neglected, for constant electrical conditions it follows that the secondary flow (represented by v^*) scales with the reciprocal of the main flow velocity U. Hence for increasing main flow velocity not only the relative importance of secondary flows is decreasing as stated by many authors but also the absolute value. 3. The second term on the right hand side shows an influence of the curvature of the main flow profile in lateral direction. This profile is mainly dominated by the effective viscosity and implies the dependence of the results to the flow model applied.

RESULTS

Qualitative Description of the Resulting Flow-Field

The results of model calculations may be presented in different ways. Fig. 3 depicts some exemplary streamlines of RANS EHD flow results. They show only small perturbations by the electrical field because the main flow is much stronger than the secondary flows, especially for U = 1 m/s. To show the *structure* of the secondary flows, one can calculate the difference of the flow fields with an applied voltage and without respectively as shown in fig. 4 for the same operating conditions as in fig. 3. This represents a fictitious flow field showing solely the secondary flows introduced by the electric field. In this representation a clear structure of the secondary flow can be observed.

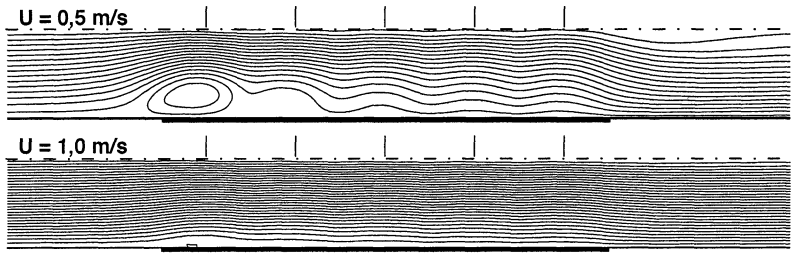

Figure 3. Streamlines of EHD flow-field for various mean flow velocities U. RANS calculations. Φ_{DE} = 50 kV

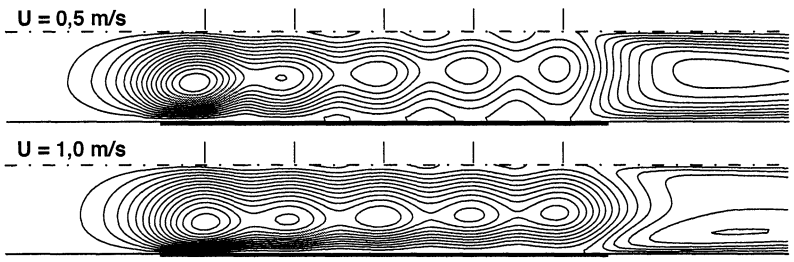

Figure 4. Streamlines of the *difference* between flows with and without applied voltage respectively. RANS calc. Φ_{DE} = 50 kV

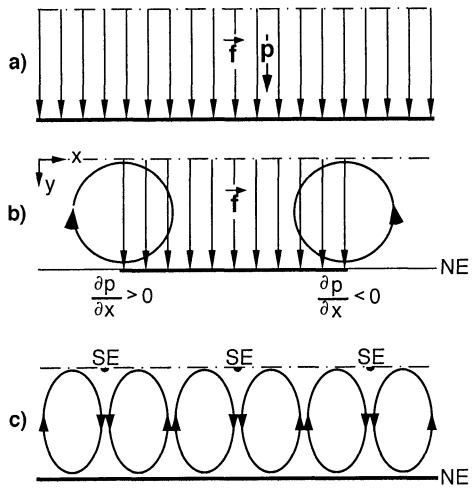

Figure 5. Schematic representation of origination of secondary flows. a) homogeneous volume force b) region of homogeneous volume force c) periodically increasing and decreasing volume forces for an infinite array of discharge electrodes.

To explain the characteristic flow pattern shown in fig. 4, some simplifying considerations are performed (see fig. 5): Considering that eq. 5 is linear in v^* and f a decomposition of the acting volume forces is applicable. If there is a homogeneous volume force throughout the channel towards the wall (e.g. homogeneous field strength and space charge) there would be no secondary flow at all, but only a pressure increase at the wall (see fig. 5a). On the other hand if this homogeneous volume force only acts in a limited region within the channel (see fig. 5b) there would be a jump of pressure at the wall leading to a clockwise vortex at the beginning of the volume force and a counterclockwise vortex at the end. Now, if we think of an infinite array of discharge electrodes (see fig. 5c) the volume force will be periodically changing, leading to a flow towards the wall, where the volume force peaks and for the sake of continuity a reverse flow, where the volume force has a minimum. This will lead to a series of clockwise and counterclockwise vortices as shown in fig. 5c.

These simplifying considerations help to explain the origination of the EHD flow pattern as exemplarily shown in fig. 4: At the beginning of the collecting electrode there is a relatively sharp increase of volume force leading to a strong clockwise vortex at the inlet. Inside the precipitator periodically increasing and decreasing volume forces are leading to flow patterns as schematically shown in fig. 5c. Due to the main flow field the strong vortex at the beginning of the collecting electrode is convected downstream superimposing with the periodically flow pattern. This will lead to an amplification of the clockwise vortices and an extinguishing of counterclockwise vortices, (compare fig. 4). At the outlet of the precipitator there is a counterclockwise vortex, but it is partially extinguished by the inlet vortex convected downstream.

All numerical model calculations published until now didn't show such strong vortices at the inlet and outlet, because these authors assumed long conducting plates with few discharge electrodes opposite the middle of the plates. Therefore the incline in volume force is more smooth and hence much weaker inlet and outlet vortices were formed (e.g. Yamamoto et al 1981 and Kallio et al., 1992). Alternatively cyclic boundary conditions are used, totally neglecting these vortices at in- and outlet (e.g. Soldati and Banerjee, 1998).

Comparison of k-ε-Calculations and Results of Perturbation Analysis

As already discussed the quite simple perturbation analysis allows many interesting conclusions concerning the evolution of EHD flow fields. Furthermore the solution of eq. 5 needs at the most 1/1000 of computational time compared to conventional RANS calculations. Therefore fig. 6 shows a comparison of results from k-ε-calculations (top picture) with results from the perturbation analysis.

Comparing the RANS calculations with the perturbation analysis when the second term on the rhs. of eq. 5 is neglected

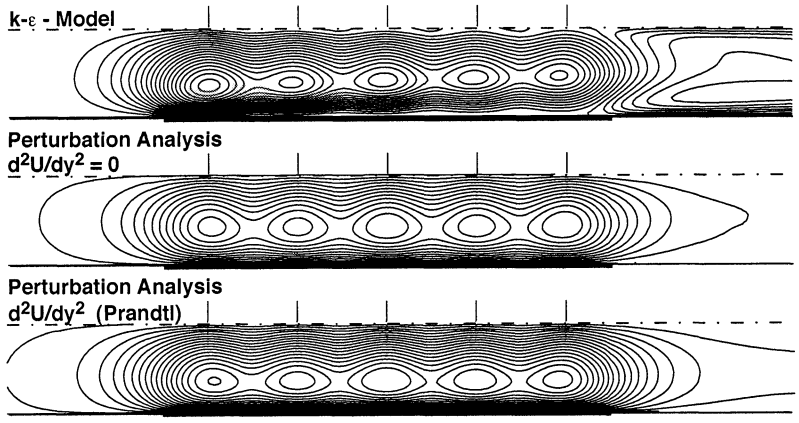

Figure 6. Isolines of streamfunction Ψ of difference between flows with and without applied voltage respectively for different flow models. Φ_{DE} = 50 kV, U = 1,0 m/s, $\Delta\Psi = 5{,}6 \cdot 10^{-4}$ m^2/s.

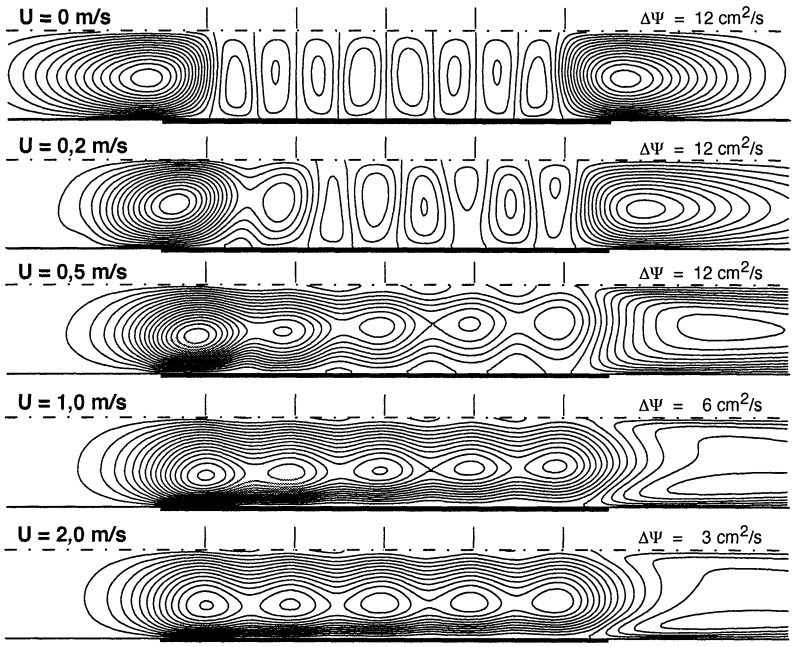

Figure 7. Isolines of streamfunction Ψ of difference between flows with and without applied voltage respectively for different main flow velocities U. Φ_{DE} = 50 kV.

(i. e. no curvature in the mean flow profile assumed) yields a quite comparable structure of the secondary flows. But they are more intense in the RANS case. Introducing the assumption of a logarithmic main flow profile according to Prandtl (Schlichting 1965) already leads to a quite good agreement qualitatively as well as quantitatively.

Hence perturbation analysis seems to be a very good means to obtain a quick estimation of the resulting secondary flows for given electric field distributions.

Influence of Main Flow Velocity

The influence of the main flow velocity on the resulting secondary flows is shown in fig. 7. If there is no main flow at all, a strong eddy at the inlet and outlet occur respectively. At each discharge electrode *two* eddies can be observed, as sketched in fig. 5c. For increasing main flow velocity one can observe the downstream convection of the eddy at the inlet little by little. For U > 0,5 m/s at each discharge electrode there is only *one* eddy left as explained above. A further increasing main flow velocity does not change the structure of the secondary flow dramatically. But comparing the distance between the streamlines $\Delta\Psi$ shows that for these velocities the secondary flows really scale as U^{-1}, as predicted by the perturbation analysis (see above).

Influence of Electrical Field Modeling

As shown in the preceding sections, the distribution of the electric field in the inlet and outlet region strongly affects the resulting flow field. Therefore in this section the influence of the electrical boundary conditions there will be discussed in more detail.

Fig. 8 compares three cases only differing in the length of the conducting collecting electrode and accordingly the electrical boundary conditions. The illustration at the top (L_0 = 5 cm) corresponds to the 'standard case' shown in all figures above. The lower illustrations show cases with collecting electrodes (and hence Dirichlet boundary conditions in electric field calculations) extended into inlet and outlet of the channel but all other geometrical parameters remained unchanged. Fig. 8 shows isoline plots and profiles of the velocity component perpendicular to the wall v which is very important in judging the influence of secondary flows on particle transport.

One can clearly recognize that the strong flow towards the center of the channel causing a deteriorative particle transport apart from the wall is heavily diminished with increasing L_0. This confirms once more the great importance of thoroughly modeling the electric field distribution. Furthermore one should always calculate the whole channel. Regarding only a part of the gap with few DE's and cyclic boundary conditions for the fluid flow seems to be not appropriate (e.g. Soldati and Banerjee 1998).

CONCLUSIONS

Some simplifying considerations can explain the resulting flow fields very well. A perturbation analysis gives a lot of information on the physics of EHD flows, inasmuch as main flow velocity, main flow profile and derivatives of volume force determine the secondary flows. Solutions of the perturbation differential equation yield good agreement with RANS calculations for much less computational effort.

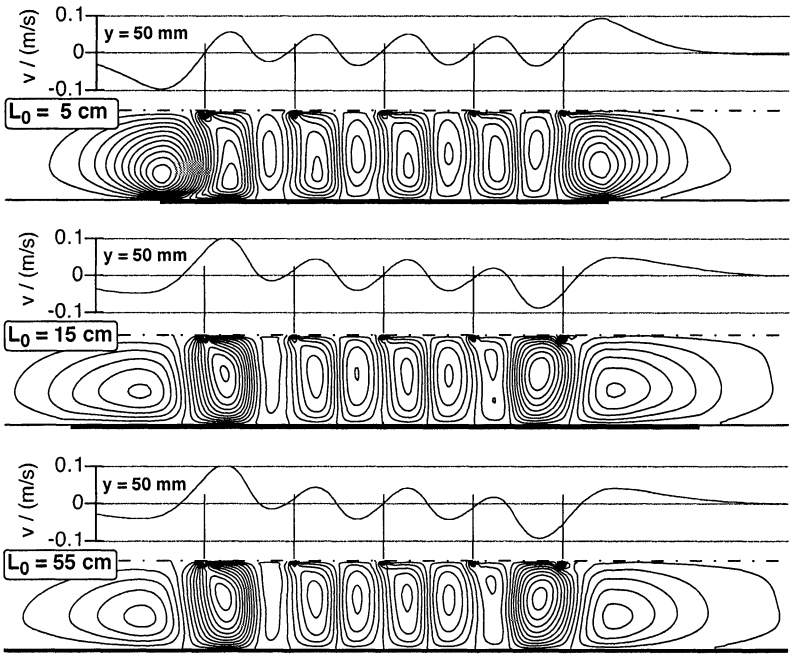

Figure 8. Isolines and profiles of velocity component perpendicular to the Wall v (positive values indicating flow towards the wall). L_0 indicating length of conducting electrode from start to fist DE (comp. fig. 2). Φ_{DE} = 50 kV, U = 1 m/s, Δv = 0,01 m/s.

The intensity of secondary flows is reversely proportional to the main flow velocity.

The resulting flow fields are very sensitive to electric field calculations. Hence high accuracy and the calculation of the whole duct with correct boundary conditions at inlet and outlet are crucial for good flow field calculations.

REFERENCES

Bernstein, S., Crowe, C.T. 1979 'Interaction between Electrostatics and Fluid Dynamics in Electrostatic Precipitators', *Environ. Intl.,* Vol. 5, pp. 181-189.

Choi, B.S., Fletcher, C.A.J. 1997 'Computation of Particle Transport in an Electrostatic Precipitator', *J. of Electrostatics,* Vol. 40/41, pp. 413-418.

Kallio, G.A., Stock, D.E. 1992 'Interaction of Electrostatic and Fluid Dynamic Fields in Wire-Plate Electrostatic Precipitators', *J. Fluid Mech.*, Vol. 240, pp. 133-166.

Launder, B.E., Spalding, D.B., 1974, 'The Numerical Computation of Turbulent Flows', *Comp. Meth. in Appl. Mech. and Eng.,* Vol. 3, pp. 269-289.

Launder, B.E., Reece, G.J., Rodi, W., 1975, 'Progress in the Development of a Reynolds-Stress Turbulence Closure. *J. Fluid Mech.*, Vol. 68, pp. 537-566.

Liang, W.-J., Lin, T.H. 1994 'The Characteristics of Ionic Wind and its Effect on Electrostatic Precipitators', *Aerosol Science and Techn.,* Vol. 20, pp. 330-344.

Medlin, A.J., Fletcher, R.H., Morrow, R. 1998, 'Electrohydrodynamic Modelling of Fine Particle Collection in Electrostatic Precipitators', *Proc. 7th Int. Conf. Electrostatic Precipitation,* Kyongju, Korea, Sept. 20-25 1998, pp. 665-672.

Meroth, A.M. 1997 'Numerical Electrohydrodynamics in Electrostatic Precipitators', Logos, Berlin.

Ramadan, O.E., Soo, S.L. 1969 'Electrohydrodynamic Secondary Flow', *Phys. Fluids,* Vol. 12, pp. 1943-1945.

Schlichting, H., 1965, 'Grenzschicht-Theorie, Braun, Karlsruhe, 5th ed., pp. 546ff.

Schmid, H.-J., 1999, 'Zum Partikeltransport in Elektrischen Abscheidern', Shaker, Aachen.

Soldati, A., Banerjee, S., 1998, 'Turbulence Modification by Large-Scale Organized Electrohydrodynamic Flows'. *Phys. Fluid,* Vol. 10, No. 7, pp. 1742-1756.

White, H.J., 1963, 'Industrial Electrostatic Precipitation', Addison-Wesley, Reading.

Yamamoto, T., Velkoff, H.R. 1981 'Electrohydrodynamics in an Electrostatic Precipitator', *J. Fluid Mech.,* Vol. 108, pp. 1-18.

ACKNOWLEDGMENTS

The authors would like to express their gratitude to Dr. Ansgar Meroth for performing the electric field calculations.

The financial support by the German Science Foundation (DFG, project No. Schm810/11-2) is gratefully acknowledged.